

## Article

# Atomic Investigation on Cold Deformation Behavior of Two Phase TiAl Polycrystalline with and without Void Defect

**Author** 

- <sup>1</sup> School of Mechanical and Electronical Engineering, Lanzhou University of Technology, Lanzhou 730050, China;  
<sup>2</sup> State Key Laboratory of Advanced Processing and Recycling of Non-ferrous Metals, Lanzhou University of Technology, Lanzhou 730050, China  
\* Correspondence: e-mail@e-mail.com; Tel.: +x-xxx-xxx-xxxx

Version October 16, 2018 submitted to Materials

**Abstract:** Fracture processes of nanocrystalline metallic materia is affected by dislocation, nano void and other defects. Existing studies of defect evolution in titanium-aluminium alloy cover the case that voids located in single crystals, inside grain in poly crystals and at the grain boundaries. Molecular dynamics simulation was performed to study the evolution of a spherical nano void in  $\alpha_2 + \gamma$  two-phase titanium-aluminium alloy under uniaxial tension. The results show that voids located at the  $\alpha_2 / \gamma$  phase boundary have significant detract to strength of Ti-Al polycrystalline.

**Keywords:**  $\alpha_2 + \gamma$  two phase TiAl alloy; void; molecular dynamics

## 1. Introduction

Ductility at room temperature and brittle rapture failure in Ti-Al alloy strongly affects the safety of fracture of structure like turbo of aircraft engine and combustion generator [1]. Deformation phenomena of TiAl alloys have been widely studied in order to overcome the problems associated with the limited ductility and damage tolerance. Much of the work has been performed on single phase  $\gamma$  alloys and PST crystals[2]. Rapture failure at the macroscopic scale can be attributed to nucleation, growth and propagation of cracks, but at the microscopic scale cracks are initially easily formed at defects in the casting process, such as voids and inclusions [3]. The initiation of crack at microscopic scale is a dynamic process, which resulting in difficulties on study of detailed mechanisms of deformation and cracking. These defects are known to play a fundamental role in the deformation of the material. It has been known that nucleation, growth and coalescence of voids are deemed as the primary mechanism of ductile material fracture, in which void growth is particularly important [4]. Therefore, it is necessary to study the deformation response of intermetallic structural materials with the consideration of microstructure evolution. A great number of literature covers a wide range of parameters such as alloy composition, microstructure and deformation temperature. Two-phase titanium aluminum alloys with proper phase distribution and grain size exhibit better mechanical performance compared with monolithic constituents  $\gamma$ (TiAl) and  $\gamma$ (Ti<sub>3</sub>Al) alloy [5]. Defects such as grain boundary, void and segregation plays an significant role in the process of fracture [6]. In order to understanding the mechanism of brittle fracture, multi-scale methods from micro to marco scale have been applied to investigate the behavior of fracture. It's necessary to carefully examine the revolution of defects and its influence on the fracture process at atomic scale. A previous study on void growth in  $\gamma$ -TiAl single crystal has reveals that void with high volume fraction detracts incipient yield strength [3]. Molecular dynamics(MD method has been use to investigate the evolution of void in materials in nanoscale [3,7,8]. The fracture mechanisms in the duplex micro-structure are plasticity induced

grain boundary decohesion and cleavage, while those in the lamellar micro-structure are interface delamination and cracking across the lamellar [3].

MD simulations has reveals that existence of voids alone may contribute to strain hardening because they are barriers to dislocation movement [9]

## 2. Molecular Dynamics Simulation

### 2.1. Atomic Potential

The interaction of particle in the material is determined by interatomic potential. Many reported examples of crack propagation in metal materials were performed with embedded atomic method due to its better accuracy in metal lattice compare with F-S and L/J [10]. The embedded atom method (MEAM) potential developed by Zope and Mishin [11] was used in the study. The simulation is submitted by MD simulations with the Large-scale Atomic/Molecular Massively Parallel Simulator (LAMMPS) open-source code [12]. We performed constant-pressure and constant-temperature (NPT) molecular dynamics simulation. The definition of potential is as following:

$$E_{total} = \sum F_i(\rho_{h,i}) + \frac{1}{2} \sum_i \sum_{j(j \neq i)} \phi_{ij}(R_{ij}) \quad (1)$$

where  $E_{total}$  is the total energy of the system,  $\rho_{h,i}$  is the host electron density at atom  $i$  due to the remaining atoms of the system,  $F_i(\rho)$  is the energy for embedding atom  $i$  into the background electron density  $\rho$ , and  $\phi_{ij}(R_{ij})$  is the core-core pair repulsion between atoms  $i$  and  $j$  separated by the distance  $R_{ij}$ . It can be noted that  $F_i$  only depends on the element of atom  $i$  and  $\phi_{ij}$  only depends on the elements of atoms  $i$  and  $j$ . The electron density is, as stated above, approximated by the superposition of atomic densities.

### 2.2. Model Creation of Crystalline

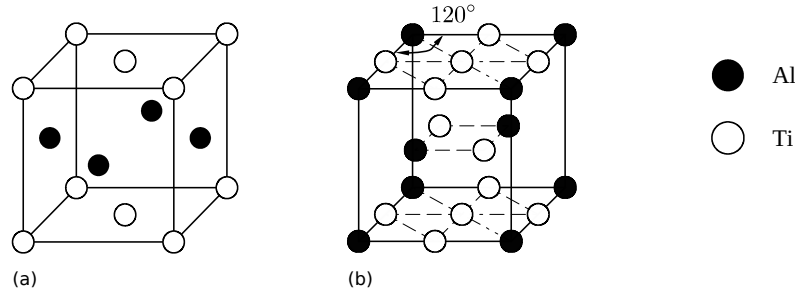


**Figure 1.** Unit cell of TiAl (a) and  $Ti_3Al$  (b)

**Table 1.** Parameters of nanocrystalline

Phase	Space group	Designation	Parameters
$\alpha_2$ - $Ti_3Al$	P6 <sub>3</sub> /mmc	0 <sub>19</sub>	$a = 0.5765$ $c = 0.46833$
$\gamma$ - TiAl	tP4	L1 <sub>0</sub>	$a = 0.3997$ $c = 0.4062$

$\gamma$  TiAl has a fcc-centered tetragonal with an L1<sub>0</sub> structure, and  $\alpha_2$  - TiAl is hcp structure, the structure of the two initial cells are shown in Fig. 5, and the constructing parameters are given by Table 1. The simulation cells of two phase polycrystalline with an initially spherical void at different position are shown in figure 2. Periodic boundary conditions (PBC) are applied along all three directions,

that makes poly crystal with periodic nanovoid structures. The initial dimension of simulation cell is  $L_x = 20 \text{ \AA}$ ,  $L_y = 18\text{\AA}$ ,  $L_z = 21 \text{ \AA}$ , and each model contains about 4.6 million atoms. The grain orientation and size were randomly created with Voronoi method with code ATOMSK [13], and resulting in the arbitrary shape and orientation of the grains. Only one spherical void defect was placed intragranularly or intergranularly within each simulation model void within each simulation model. The intragranular spherical void was located in grain interior of the largest grain of the simulation model, as shown in Fig. 2(b). The intergranular spherical void was at the center of the simulation cell, as shown in Fig. 2(d).

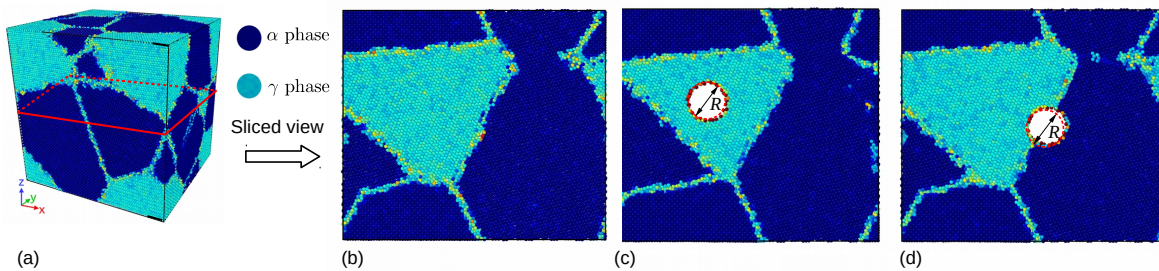


**Figure 2.** Model creation: without void defect(b);with intergranular void(c), with inergranular void(d)

### 2.3. Analysis method

The centrosymmetry parameter is defined as follow:

$$P = \sum_{i=1}^6 |\vec{R}_i + \vec{R}_{i+6}|^2 \quad (2)$$

where  $\vec{R}_i$  and  $\vec{R}_{i+6}$  are the vectors corresponding to the six pairs of opposite nearest neighbors in the fcc lattice. The centrosymmetry parameter(CSP) is zero for atoms in a perfect lattice. In other words, if the lattice is distorted the value of P will not be zero. Instead, the parameter will have a value within the range corresponding to a particular defect. By removing all the perfect and surface atoms within the bulk, the existence of dislocation atoms become visible.

## 3. Results and Discussion

In order to examine deformation behaviour carefully, tensile loading was applied to the model without any types of void defect. The whole tension process was separated into four stages: Stage-I is typical elastic part of the deformation, which is originated from  $\epsilon = 0$  to  $\epsilon = 0.092$ , including key point 1. Stage-II is yield stage ranging from  $\epsilon = 0.092$  to  $\epsilon = 0.101$ , including key points 2 to 6. In stage-II, the stress decreased slightly along with the increasing of strain. Stage-III is cracking stage and in this stage the strength of the model have been detracted sharply, we can confine that the structure almost fail after the Stage-III. Snapshots of atoms configuration are labeled with key points number from 1 to 10, specific list of key points numbers were shown in Table. 2. Deformation behaviour of the  $\alpha_2$  phase had  $\gamma$  phase were discussed in the following subsection respectively.

**Table 2.** Key point during tensile process

Key Number	1	2	3	4	5	6	7	8	9	10
Time/ps	0	0.15	0.16	0.17	0.18	0.19	0.20	0.21	0.22	0.23
Strain	0	0.092	0.094	0.096	0.099	0.101	0.104	0.107	0.110	0.112

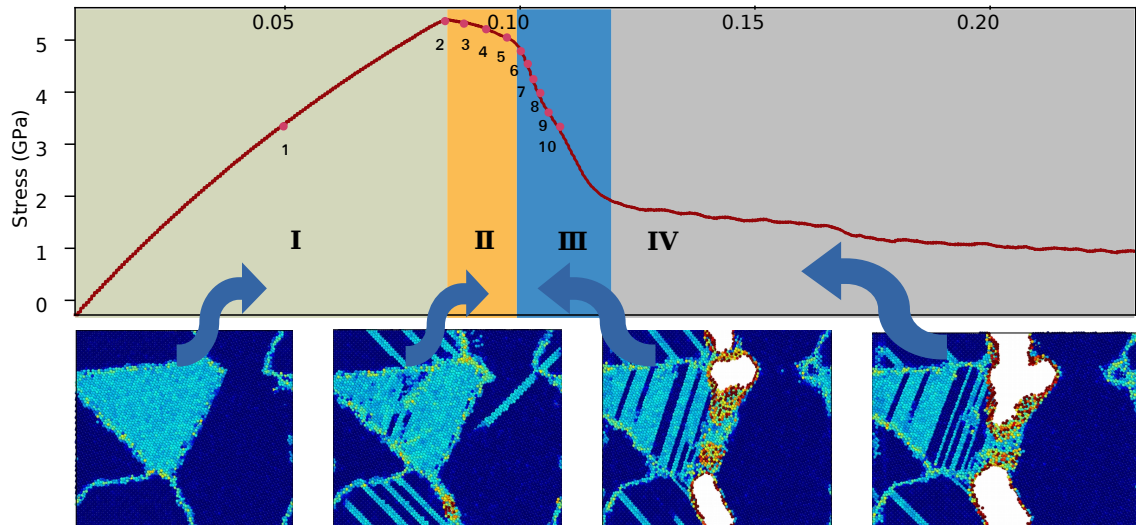


**Figure 3.** Deformation process of the model without void defect

### 3.1. Deformation Behaviour of Two Phase Alloys without Void Defects

However, the following discussion concentrates on deformation phenomena that rely on the elastoplastic codeformation of the  $\gamma$  and  $\alpha_2$  phases and on the particular point defect situation occurring in twophase alloys. Due to this effect ( $\alpha_2 + \gamma$ ) alloys exhibit some remarkable properties that are unlike those of either constituent.

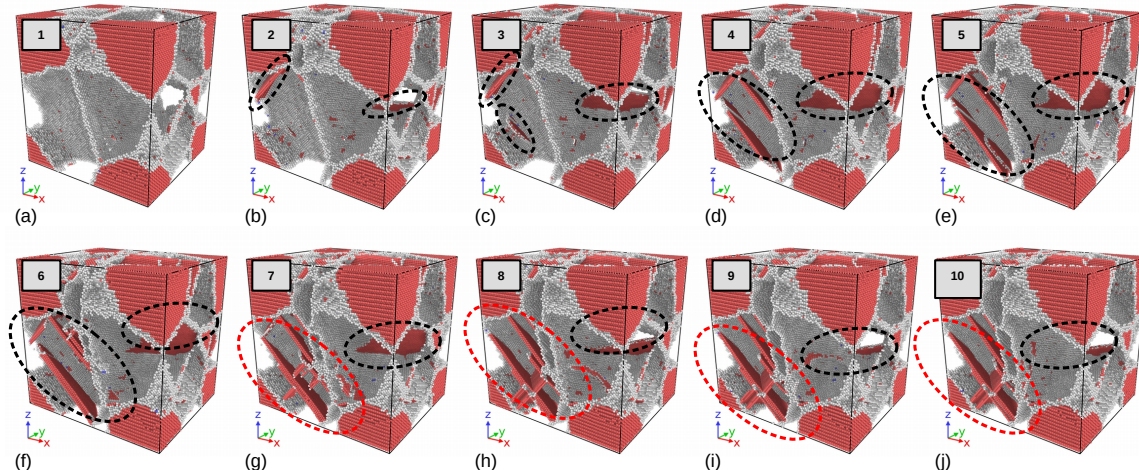


**Figure 4.** Defect evolution in  $\gamma$  phase (perfect atoms of  $\alpha$  phase have been removed)

The configuration of atoms is shown in Fig. 9, it can be seen that dislocation emission initiate in  $\gamma$  phase in XXX ps, and the deformation can be mainly confined to the majority  $\gamma$  phase.  $\gamma$ (TiAl) deforms by octahedral glide of ordinary dislocations with the Burgers vector  $b = 1/2 < 110 \bar{1}$  and superdislocations with the Burgers vectors  $b = < 101 \bar{1} \bar{1}$  and  $b = 1/2 < 11\bar{2}$ . The other potential deformation mode is mechanical twinning along  $1/6 < 11\bar{2} 111$ .

From Fig. 9, of the two constituents of  $(\alpha_2 + \gamma)$  alloys, the  $\alpha_2$  phase is more difficult to deform. A reason for the unequal strain partitioning between the  $\alpha_2$  and  $\gamma$  phase is certainly the strong plastic anisotropy of the  $\alpha_2$  phase. TEM examinations performed on tensile tested lamellar alloys have revealed that the limited plasticity of the  $\alpha_2$  phase is mainly carried by local slip of  $<\mathbf{a}>$ -type dislocations with the Burgers vector  $b = 1/3 < 11\bar{2}0 >$  prism planes<sup>9</sup>, which is by far the easiest slip system in  $\alpha_2$  single crystals.

### 3.2. Model Creation of Crystalline

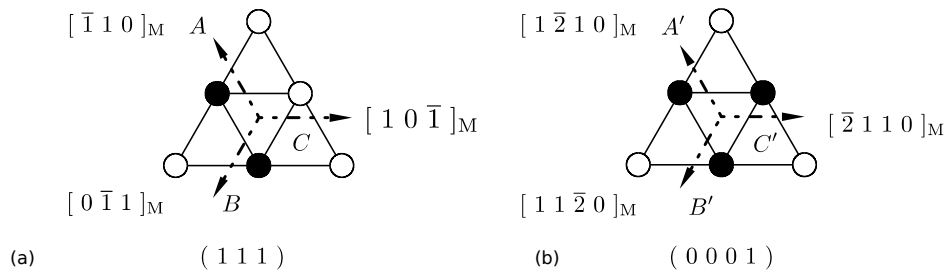


**Figure 5.** close packed plane of  $\gamma$  phase (TiAl) and  $\alpha$ (Ti<sub>3</sub>Al) phase

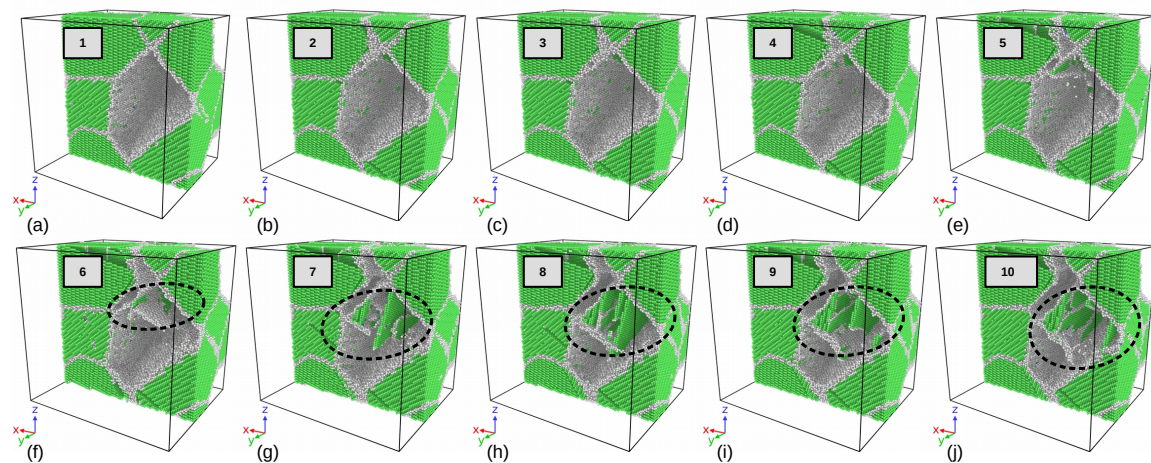


**Figure 6.** Defect evolution in  $\alpha_2$ -phase (perfect atoms in  $\alpha_2$  phase have been removed)

In many cases the orientation of slip slip is changed because the crystallographically available slip and directions are not continuous across the interface. This may significantly reduce the Schmid factor and thus impede slip transfer. At the  $\gamma/\gamma$  interfaces the orientation of the slip plan could change through a relevantly large angle of about 90 degree. Reorientation of slip is always required at the  $\alpha_2/\gamma$  interface; the smallest angle between the corresponding slip planes  $111_\gamma$  and  $10 - 10_{\alpha_2}$  is about 19 degree [1].

The core of a dislocation intersecting an interface often needs to be transformed. For example, an ordinary  $1/2<110]$  dislocation gliding in one  $\gamma$  grain has to be converted in to a  $<101]$  super dislocation with the double Burgers vector gliding in an adjacent  $\gamma$  grain. At the  $\alpha_2/\gamma$  interface the dislocations existing in the  $D0_{19}$  structure have to be transformed into dislocations consistent with the  $L1_0$  structure. These core transformations are associated with a change of the dislocation line energy because the lengths of the Burgers vectors and the shear module are different.

Dislocations crossing semi-coherent boundaries have to intersect the misfit dislocations, a process that involves elastic interaction, jog formation and the incorporation of gliding dislocations into the mismatch structure of the interface. When the slip is forced to cross  $\alpha_2$  lamella, pyramidal slip of the  $\alpha_2$  phase is required, which needs an extremely high shear stress.

### 3.3. Evolution of spherical void in the simulation with intragranular spherical voids

The volume defects considered pertain to three-dimensional objects contained within a matrix. Three-dimensional structures composed of zero-, one- or two-dimensional defects are not considered here. Second-phase particles, precipitated within, as a consequence of a thermal treatment, or taken up, as a consequence of a material processing route, into a matrix of the first, dominant phase, disrupt,

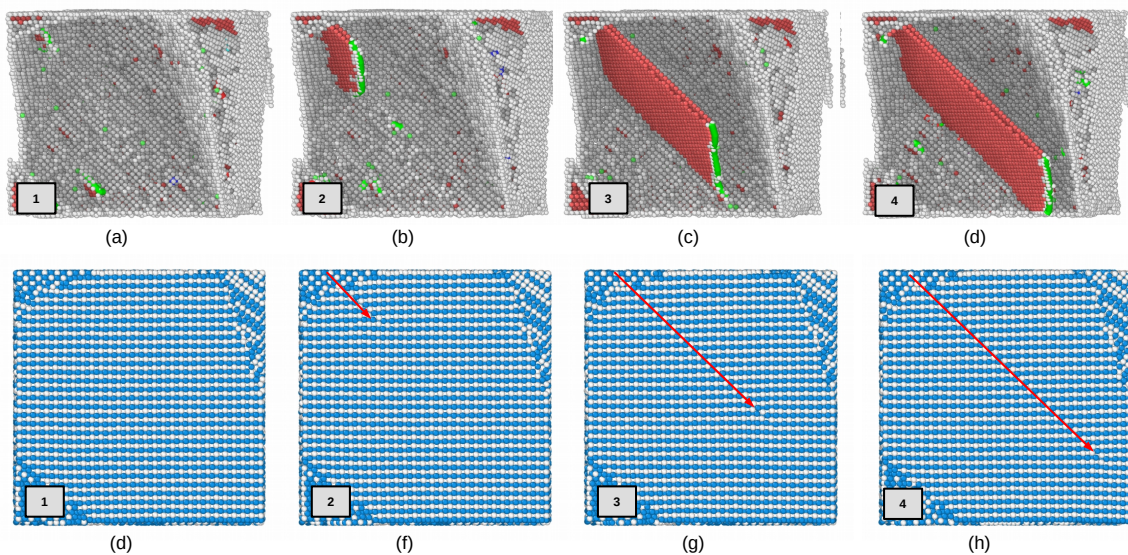


**Figure 7.** Dislocation in  $\gamma$

more or less (as possibly associated with the occurrence of incoherent or coherent interfaces; see Sect. 5.3), the long-range translation symmetry of the matrix. They may induce considerable misfit-stress fields and thus can influence material properties pronouncedly. Such stress fields surrounding the second-phase particles can be due to misfit between the volume occupied by the second-phase particle when unconstrained and the space ("hole") put at its disposal by the matrix. Such misfit can arise due to specific volume differences induced by precipitation or by different thermal expansion or shrinkage upon heating or cooling the specimen. A possibly favorable effect of second-phase particles is a contribution to the enhancement of mechanical strength. Considering yielding of a material as related to glide of dislocations (Sect. 5.2.5), any mechanism obstructing dislocation glide improves the mechanical strength. In the discussion of the Frank–Read source for dislocation (-line) production (Sect. 5.2.6) it was made clear that second-phase particles can serve as obstacles for dislocation migration: the stress fields surrounding the second-phase particles can be of "antagonistic" nature and "block" propagation of the stress field of a migrating dislocation: the second-phase particle acts as "pinning point". It was already indicated that in order that a dislocation can pass two pinning points (A and B in Fig. 5.13; see Sect. 5.2.6) a critical shear stress is needed that depends on the distance between the obstacles (which can be second-phase particles):

$$\tau_0 = Gb/d \quad (3)$$

where  $d$  represents the distance between A and B and thus reflects the dependence of the critical shear stress  $\tau_0$  on the second-phase particle density and distribution. This mechanism for hardening is designated as the Orowan process (with  $\tau_0$  as the Orowan (shear) stress ; sgitee also Sect. 11.14.4). As a result of the Orowan process, upon passage of the pinning points by a series of gliding dislocations, a system of concentric loops is formed around the second-phase particles (see Fig. 5.27). Consequently, the effective average distance between the second-phase particles has decreased to  $d$  which implies a necessary increase of the value of critical shear stress required for continuation of dislocation glide (cf. (5.10)). A step, of the width of a burgers vector, will be generated at both sidesof a crystal along the direction of the burgers vector after dislocation traversing the entire crystal, as is shown in 8. A small tep will be formed at spherical void surface toward the void interiorafter dislocation absorption at spherical void surfaces. If a great number of dislocation slip along their respective systemstowards the spherical nano void in all directions, and are absorbed at the spherical void surfaces, the spherical nano void will eventually shrink from the dash circle to

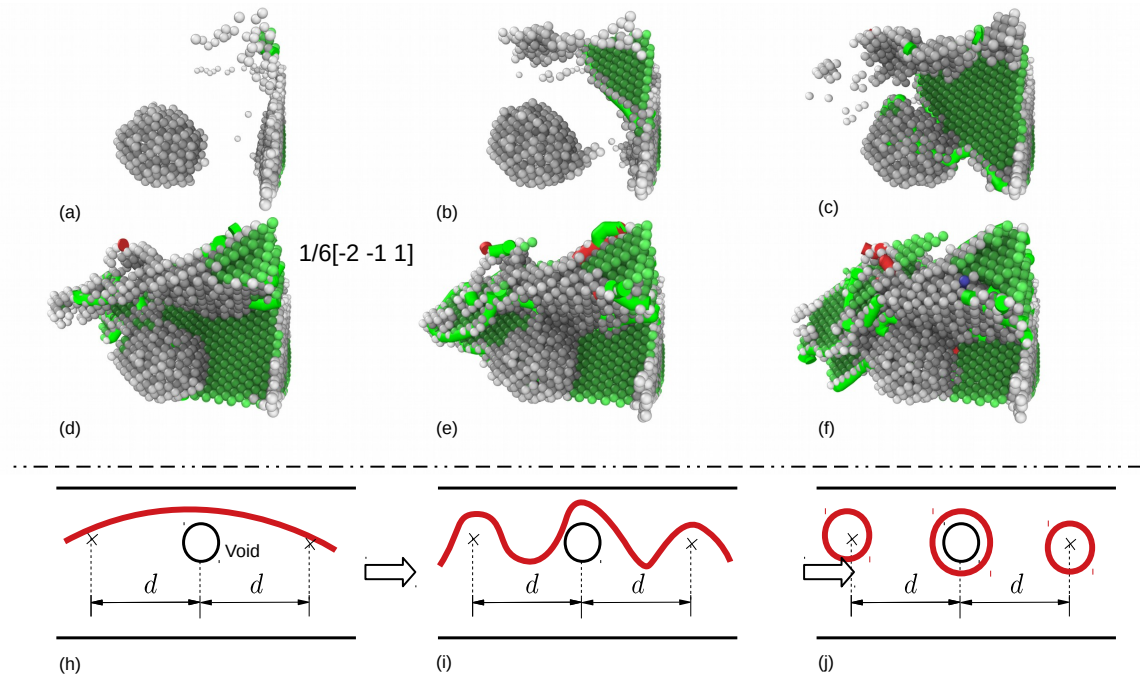


**Figure 8.** Orowan process in  $\alpha$ -phase ( $\alpha$  phase atoms have been removed)

### 3.4. The effect of void on the strength of material

Void of  $R=10 \text{ \AA}$  was placed at phase boundary, inside  $\alpha_2$  phase grain respectively. Effect of void at different position under uniaxial tension is shown in Fig.10. The strength of materials with void in different size and at different position is shown in Fig.10. The results show that the model without void defect has best strength, while the void located inside  $\alpha_2$  phase detracts the strength of the material most, and the void at phase boundary have less impact on the strength.

The effect of size is expectable that the greater voids detracts the strength of the materials more, however, it has been observed in the simulation that there is a critical value about  $15\text{\AA}$  for voids at different position. The voids larger than  $15\text{\AA}$  have dramatic detraction to the strength of the material. Conventional definition of strength of materials with geometry subtraction was applied to the model, and theoretical strength of the models was calculated by formulation 4:

$$\sigma^* = \sigma_0 \cdot \frac{A^*}{A_0} \quad (4)$$

where  $\sigma_0$  is the strength of the model without void defects  $5.26 \text{ Gpa}$ , and  $A_0$  is initial section area,  $A = 36000 \text{ \AA}^2$ ,  $A^*$  is section area in consider of the subsection that results from the voids. Comparing with the strength determined by molecular dynamics simulation and the results calculated with formulation 4, it can be assumed that the main factor that affects the strength of materials can be attributed to local behaviour of the materials, thus revolution of defects should be examined carefully.

Voids with different size:  $2\text{\AA}$ ,  $5\text{\AA}$ ,  $10\text{\AA}$ ,  $15\text{\AA}$  were placed into the model respectively. It has been observed that voids detracts the strengths of the material. The max stress stress of the simulation cell decreases as the volume of voids are lareger. From Fig 10, there is a critical value of void radius about  $15\text{\AA}$ , the void greater than  $15\text{\AA}$  cause serious detraction of strength of material. Engineering stress is calculated

$$\sigma = S / A$$

The rate of decrease of loading area are smaller comparing with the detraction of strength, so it can be assumed that the yield yield behaviour and strength is much more related with local behaviour of grain boundaries and void.

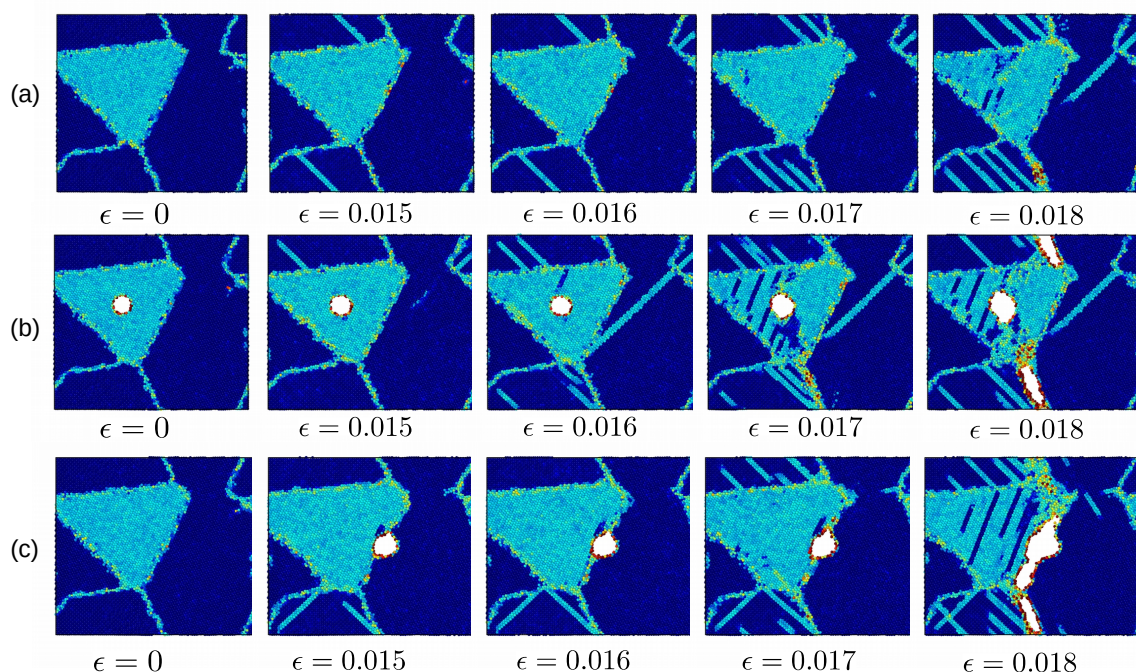


**Figure 9.** Yield process of the models

Grain and phase boundaries are obstacles to deformation process, thus the stability of boundaries have great impact on the strength of materials. Interaction between grain boundary and void determines the fracture mode of the TiAl alloy.

According to Schmid's law:

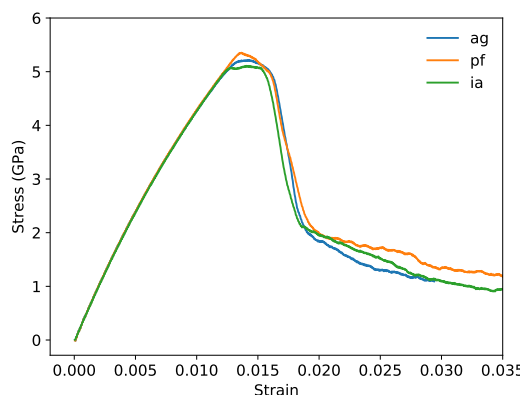
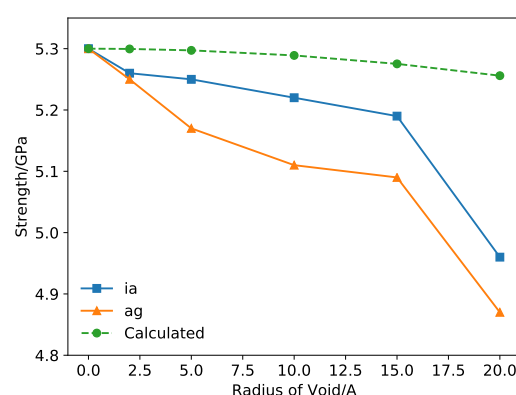
$$\tau = \sigma * m$$

where  $m$  is the Schmid factor :

$$m = \cos(\phi)\cos(\lambda)$$

## References

1. Munz, E.D. Psychotherapie in der Psychiatrie. *Nervenheilkunde* **2017**, *36*, 800–805, [[arXiv:1011.1669v3](https://arxiv.org/abs/1011.1669v3)]. doi:10.1007/s13398-014-0173-7.2.
2. Appel, F.; Clemens, H.; Fischer, F.D. Modeling concepts for intermetallic titanium aluminides. *Progress in Materials Science* **2016**, *81*, 55–124. doi:10.1016/j.pmatsci.2016.01.001.
3. Tang, F.L.; Cai, H.M.; Bao, H.W.; Xue, H.T.; Lu, W.J.; Zhu, L.; Rui, Z.Y. Molecular dynamics simulations of void growth in  $\gamma$ -TiAl single crystal. *Computational Materials Science* **2014**, *84*, 232–237. doi:10.1016/j.commatsci.2013.12.014.
4. Hempel, N.; Bunn, J.R.; Nitschke-Pagel, T.; Payzant, E.A.; Dilger, K. Study on the residual stress relaxation in girth-welded steel pipes under bending load using diffraction methods. *Materials Science and Engineering A* **2017**, *688*, 289–300. doi:10.1016/j.msea.2017.02.005.
5. Kim, Y.W. Effects of microstructure on the deformation and fracture of  $\gamma$ -TiAl alloys. *Materials Science and Engineering: A* **1995**, *192-193*, 519–533. doi:10.1016/0921-5093(94)03271-8.
6. Larsen, P.M.; Schmidt, J. Robust structural identification via polyhedral template matching. *Modelling and Simulation in Materials Science and Engineering* **2016**, *24*, 055007, [[1603.05143](https://arxiv.org/abs/1603.05143)]. doi:10.1088/0965-0393/24/5/055007.
7. Jing, P.; Yuan, L.; Shivpuri, R.; Xu, C.; Zhang, Y.; Shan, D.; Guo, B. Evolution of spherical nanovoids within copper polycrystals during plastic straining: Atomistic investigation. *International Journal of Plasticity* **2018**, *100*, 122–141. doi:10.1016/j.ijplas.2017.09.016.

**Figure 10.** Stress-Strain**Figure 11.** Strength of models

8. Elkhateeb, M.G.; Shin, Y.C. Molecular dynamics-based cohesive zone representation of Ti6Al4V/TiC composite interface. *Materials and Design* **2018**, *155*, 161–169. doi:10.1016/j.matdes.2018.05.054.
9. Xiong, L.; Xu, S.; McDowell, D.L.; Chen, Y. Concurrent atomistic-continuum simulations of dislocation-void interactions in fcc crystals. *International Journal of Plasticity* **2015**, *65*, 33–42. doi:10.1016/j.ijplas.2014.08.002.
10. Ko, W.S.; Grabowski, B.; Neugebauer, J. Development and application of a Ni-Ti interatomic potential with high predictive accuracy of the martensitic phase transition. *Physical Review B* **2015**, *92*, 134107. doi:10.1103/PhysRevB.92.134107.
11. Zope, R.R.; Mishin, Y. Interatomic potentials for atomistic simulations of the Ti-Al system. *Physical Review B - Condensed Matter and Materials Physics* **2003**, *68*, 024102, [arXiv:cond-mat/0306298]. doi:10.1103/PhysRevB.68.024102.
12. Plimpton, S. Fast parallel algorithms for short-range molecular dynamics. *Journal of Computational Physics* **1995**, *117*, 1–19, [arXiv:10.1002/nag.2347]. doi:10.1006/jcph.1995.1039.
13. Hirel, P. Atomsk: A tool for manipulating and converting atomic data files. *Computer Physics Communications* **2015**, *197*, 212–219. doi:10.1016/j.cpc.2015.07.012.

© 2018 by the authors. Submitted to *Materials* for possible open access publication under the terms and conditions of the Creative Commons Attribution (CC BY) license (<http://creativecommons.org/licenses/by/4.0/>).